

# Polymer translocation through extended patterned pores in two dimensions: Scaling of the total translocation time

Andri Sharma<sup>1,2,\*</sup>, Abhishek Chaudhuri<sup>1,†</sup> and Rajeev Kapri<sup>1‡</sup>

<sup>1</sup> Department of Physical Sciences, Indian Institute of Science Education and Research (IISER) Mohali, Sector 81, S. A. S. Nagar 140306, Mohali, Punjab, India and

<sup>2</sup> National Centre for Biological Sciences-TIFR, Bellary Road, Bengaluru 560065

We study the translocation of a flexible polymer through extended patterned pores using molecular dynamics (MD) simulations. We consider cylindrical and conical pore geometries that can be controlled by the angle of the pore apex  $\alpha$ . We obtained the average translocation time  $\langle\tau\rangle$  for various chain lengths  $N$  and the length of the pores  $L_p$  for various values  $\alpha$  and found that  $\langle\tau\rangle$  scales as  $\langle\tau\rangle \sim N^\gamma \mathcal{F}(L_p N^\phi)$  with exponents  $\gamma = 3.00 \pm 0.05$  and  $\phi = 1.50 \pm 0.05$  for both patterned and unpatterned pores, respectively.

## I. INTRODUCTION

Polymer and protein translocation through narrow pores is a fundamental process in biology and an emerging paradigm for nanoscale transport in technology. Translocation of polymer or proteins is an ubiquitous process inside biological cells and is among one of the important processes that propel the cell functionality [1, 2]. In the past two and half decades, polymer translocation has gained considerable attention due to its technological applications such as rapid DNA sequencing, gene therapy and controlled drug delivery [3, 4]. Recent advances in nanofabrication have enabled stable synthetic nanopores that can operate under high voltages, elevated temperatures, and various solvent conditions. These pores have become controllable experimental systems to explore the physics of single-molecule transport. A single strand of a biopolymer such as DNA or RNA can be electrophoretically driven through such nanopores in a controlled manner. The ion current flowing through the nanopore gets blocked when the polymer is inside the pore which gives the signature of the polymer sequence [5].

The translocation of polymer through nanopores depends on various parameters, such as, the length of the polymer chain, its structure, shape and the size of the pore and pore-polymer interactions [6, 7]. Consequently, polymer translocation is a complex, system-dependent nonequilibrium process whose understanding requires both theoretical modelling and computational simulations. Various coarse-grained models have been used to understand the translocation phenomenon [7–14]. For example, the translocation process has been studied as a one-dimensional barrier crossing problem of the translocation coordinate through a slit (i.e., a pore of unit length). In initial studies, it was assumed that the translocation time is long enough to ensure the equilibration of the polymer conformations at every stage of the translocation process [7, 8, 15]. Later, a ma-

jority of experimental studies with synthetic nanopores showed that the time taken by the polymer to pass the nanopore is much less than its relaxation time, indicating that translocation is a non-equilibrium process. The tension propagation (TP) theory proposed originally by Sakaue [11] for an infinite chain and subsequently modified by Ikonen et al. [14, 16–18] and Dubbeldam et al. [19] for finite chains has proven to be successful in explaining the non-equilibrium aspect of driven polymer translocation [20]. The most important quantity of interest in polymer translocation studies is the dependence of the average translocation time,  $\langle\tau\rangle$ , on the chain length  $N$ . Numerical simulations and experiments have indicated that  $\langle\tau\rangle \sim N^\beta$ . Different values of  $\beta$  have been observed in different studies, suggesting that  $\langle\tau\rangle$  depends on various physical parameters [21]. For a self-avoiding flexible chain,  $\langle\tau\rangle$  is known to scale as  $\langle\tau\rangle \sim N^{1+\nu}$ , here  $\nu = 3/4$  in two dimensions [18, 22, 23], and  $\nu \approx 0.59$  in three dimensions [12, 22, 24].

While early theoretical work considered a very short or unit-length pore, most realistic nanopores are extended and of finite length, often with diameters of tens of monomer long. In such pores, the details of the pore–polymer interaction and spatial patterning along the pore axis strongly influence the dynamics [25–29]. There have been theoretical and computational studies on finite-length pores where the shape of the extended pore is cylindrical, with different patterned pore–polymer interactions [23, 30–34], or conical [35–41]. For cylindrical pores, it was estimated that for a fixed external drive  $\langle\tau\rangle$  depends on the patterning of the pores. It was found that  $\langle\tau\rangle$  is the maximum for a fully attractive pore and is the minimum for a pore having a repulsive exit [32, 34]. It was argued that the pattern stickiness of extended pores can be exploited to predict heteropolymer sequences with different bending rigidities to a high degree of accuracy by translocating them through multiple pores [34]. For conical pores, we have one more parameter—the cone apex angle, which we represent by  $\alpha$ . For  $\alpha = 0$ , we have a cylindrical pore. For a conical pore with attractive pore–polymer interactions,  $\langle\tau\rangle$  was found to be a non-monotonic function of  $\alpha$  for lower driving forces, which becomes monotonic for higher forces [38, 39].

\* sharmaandri1@gmail.com

† abhishek@iisermohali.ac.in

‡ rkapri@iisermohali.ac.in

The length of the extended pore,  $L_p$ , introduces a second independent length scale in addition to the polymer contour length  $N$ . Understanding how these two compete under different interaction patterns is essential for controlling transport through synthetic or biological nanopores. Although there have been many scaling studies of  $\langle \tau \rangle$  on the length of the polymer  $N$ , not much is discussed in the literature on the dependence of  $\langle \tau \rangle$  on  $L_p$ . We try to address this in this paper.

In this work we use two-dimensional Langevin dynamics simulations to study the driven translocation of a flexible polymer through extended conical pores having different attractive–repulsive patterns. The two-dimensional approach enables long-chain statistics and extensive averaging, while retaining the essential physics of polymer stretching and confinement. We extend our work on conical pores [38, 39] to study the effect of different pore patterns on the driven-translocation process. The patterning is created along the pore length by having various sections with attractive and repulsive interactions. The entrance of the pores is always attractive, so that the polymer can enter the pore with ease. The exit from the pore can either be attractive or repulsive. The presence of an external drive along the channel often facilitates the translocation process. We present our study on translocation behavior by varying the pore length  $L_p$  and the polymer length  $N$ . The key questions we address are: (i) how does the mean translocation time depend simultaneously on  $N$  and  $L_p$ , and (ii) whether distinct pore patterns produce universal or pattern-specific scaling behavior.

The rest of this paper is organized as follows. In Sec. II, we define our model and simulation details. In Sec. III, we study the effect of the pore length,  $L_p$ , and chain length,  $N$ , on  $\langle \tau \rangle$ . We also discuss the effect of patterned pores on  $\langle \tau \rangle$  and establish scaling relations between  $\langle \tau \rangle$ ,  $L_p$  and the polymer length  $N$  for extended pores. In Sec. IV, we conclude by providing a discussion of the obtained scaling exponents.

## II. MODEL

All simulations are performed in two dimensions (2D). The reduced dimensionality allows extensive statistical sampling and direct comparison with earlier 2D translocation studies [22, 23]. The essential physics of polymer stretching and confinement within narrow pores remains captured in 2D while significantly lowering computational cost.

The polymer is modeled as a bead-spring chain [42], where the consecutive beads with diameter  $\sigma$  are connected with a spring of spring constant  $K$  interacting via a harmonic potential given by:

$$U_{\text{bond}} = \frac{1}{2}K(r - r_0)^2, \quad (1)$$

where  $r_0 = 1.0\sigma$  is the equilibrium bond length. The non-

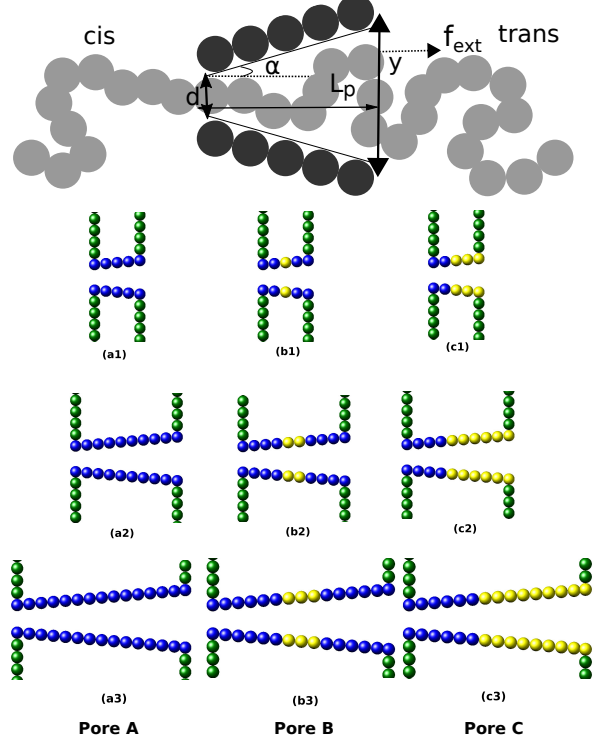


FIG. 1. Top row shows a schematic diagram of pore-polymer set up for translocation in two-dimensions. The pore is 5 beads long with a half apex angle  $\alpha$ . The pore diameter on the cis end is  $d = 2.25\sigma$ , whereas it is  $y = d + 2L_p \tan \alpha$  on the trans end. The flexible polymer is made up of beads with diameter  $\sigma = 1$  connected with springs. The subsequent rows show patterned pores with different pore lengths,  $L_p = 5, 10$ , and  $15$ , respectively. The blue beads are attractive while the yellow and green beads are repulsive in interaction with polymer chain.

bonded polymer beads interact via the Weeks-Chandler-Andersen (WCA) potential  $U_{\text{nb}}(r)$  of the form:

$$U_{\text{nb}}(r) = \begin{cases} 4\epsilon \left[ \left(\frac{\sigma}{r}\right)^{12} - \left(\frac{\sigma}{r}\right)^6 \right] + \epsilon, & r < r_{\min} \\ 0, & r \geq r_{\min}, \end{cases} \quad (2)$$

where  $\epsilon$  is the strength of the potential. The cutoff distance  $r_{\min} = 2^{1/6}\sigma$  is set at the minimum of the potential. Unless otherwise stated, we set  $\epsilon = 1.0$  and use the same energy scale for all interactions.

The pores are static and are constructed with coarse-grained beads of size  $\sigma$ . We study three different types of extended pores as considered in Ref. [34]:

- (1) Pore A is an attractive pore. Polymer beads interact with pore beads via the attractive Lennard-

Jones (LJ) potential,  $U_{\text{pp}}(r)$ :

$$U_{\text{pp}}(r) = \begin{cases} 4\epsilon_p \left[ \left(\frac{\sigma}{r}\right)^{12} - \left(\frac{\sigma}{r}\right)^6 \right], & r < r_c \\ 0, & \text{otherwise,} \end{cases} \quad (3)$$

where  $\epsilon_p = 1.5\epsilon$  is the attractive strength of the pore and  $r_c = 2.5\sigma$  is the cut-off distance.

(2) Pore B has attractive entrances and exits separated by a repulsive section. The polymer beads interact with attractive beads of the pore via the LJ potential and with beads of the repulsive section via the WCA potential.

(3) Pore C has an attractive entrance and a repulsive exit. The polymer beads interact with the beads of the attractive section of the pore via the LJ potential and the beads of the repulsive section via the WCA potential.

The entrance of all pores is kept attractive to ensure capture of the polymer, while the exit region determines the ease of release. The total pore pattern is scaled proportionally when the pore length  $L_p$  is varied so that the relative fraction of attractive and repulsive segments remains constant.

In addition to the above potentials, an external pulling force,  $\vec{f}_{\text{ext}}$ , which mimics an electrophoretic drive, is applied inside the pore in the positive  $x$ -direction to ensure that the polymer translocates through the pore from the *cis* to the *trans* side. The force magnitude varies along the pore extension as

$$f_{\text{ext}}(x) = \frac{f_0 d}{(d + 2x \tan \alpha)}, \quad (4)$$

where  $f_0$  is the driving force at the pore entrance of width  $d$ . For a conical pore ( $\alpha > 0$ ), this form maintains a constant total integrated force along the pore length, causing the local field to decrease gradually from the entrance to the exit. For  $\alpha = 0^\circ$ , the same equation reduces to a constant field in a cylindrical pore, as expected. The schematic diagram of our coarse-grained model is shown in Fig. 1 (top row). The subsequent rows show the schematic diagram of three different pore patterns that we study in this paper. The second row shows three different patterned pores for length  $L_p = 5$ : Fig. 1(a1) corresponds to a fully attractive pore (Pore A), Fig. 1(b1) shows a pore with attractive entrances and exits but a repulsive middle segment (Pore B), and Fig. 1(c1) shows a pore with an attractive entrance and a repulsive exit (Pore C). In the third and fourth rows, we show pores for lengths  $L_p = 10$  and  $L_p = 15$ , respectively.

The dynamics of the polymer is governed by the stochastic Langevin equation. The equation of motion for the position of the  $i$ th monomer is

$$m\ddot{\vec{r}}_i = -\eta\dot{\vec{r}}_i - \nabla_i(U_{\text{bond}} + U_{\text{nb}} + U_{\text{pp}}) + \vec{f}_{\text{ext}} + \vec{\zeta}_i, \quad (5)$$

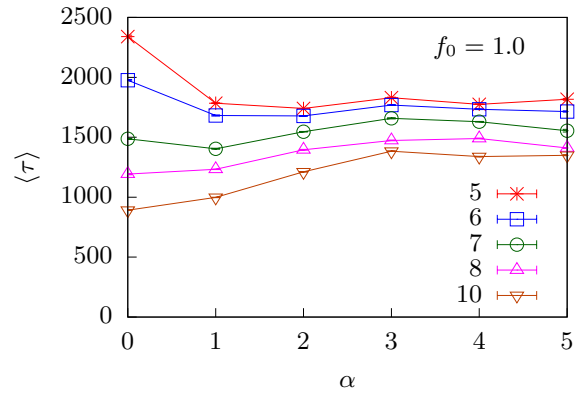


FIG. 2. Plots showing the variation of  $\tau$  vs.  $\alpha$  behavior, with the change of pore-length,  $L_p$ . Here, the polymer is flexible with length  $N$  of 128 beads, and pore-length varies from  $5\sigma$  to  $10\sigma$ .

where  $m$  and  $\vec{r}_i$  are the mass and position of the  $i$ th bead, respectively,  $\eta$  is the friction coefficient of the fluid, and  $\vec{\zeta}_i$  is a random Gaussian noise obeying the fluctuation-dissipation relation  $\langle \zeta_{i\mu}(t)\zeta_{j\nu}(t') \rangle = 2k_B T \eta \delta_{ij} \delta_{\mu\nu} \delta(t - t')$ .

In our model,  $\epsilon$ ,  $\sigma$  and  $m$  set the units of energy, length, and mass, respectively. This sets the unit of time as  $(m\sigma^2/\epsilon)^{1/2}$ . The force value is set in units of  $\epsilon/\sigma$  and the spring constant in units of  $\epsilon/\sigma^2$ . Using this system of units, the dimensionless parameters  $k_B T = 1$ ,  $\eta = 1$ ,  $d = 2.25$ , and  $K = 500$  are chosen in the simulations. The choices of  $\eta$  and  $d$  follow standard coarse-grained studies [30, 32], ensuring realistic frictional damping and pore geometry comparable with experimental nanopores.

For every simulation data point, the results are averaged over 1500–2000 successful translocation events. Error bars representing one standard error of the mean are shown in all plots. Molecular-dynamics trajectories are obtained using LAMMPS [43] software.

### III. RESULT AND DISCUSSION

#### A. Effect of pore length

The length of the pores,  $L_p$ , plays an important role in the translocation of a polymer through a membrane channel. To study how the translocation time depends on the length of the pores, we consider a polymer of length  $N = 128$  and translocate it through pores of varying lengths  $L_p \in [5\sigma, 10\sigma]$ . (Error bars in all figures denote one standard error based on 1500–2000 successful events.) For each pore length, we also vary the angle of the cone apex,  $\alpha$ , in the range  $\alpha \in [0, 5]$  degrees. The magnitude of the external force is kept constant at  $f_0 = 1$ . The pore-polymer interaction is attractive in nature and is modeled using Eq.(3). In Fig. 2, we have plotted the average translocation time  $\langle \tau \rangle$  as a function

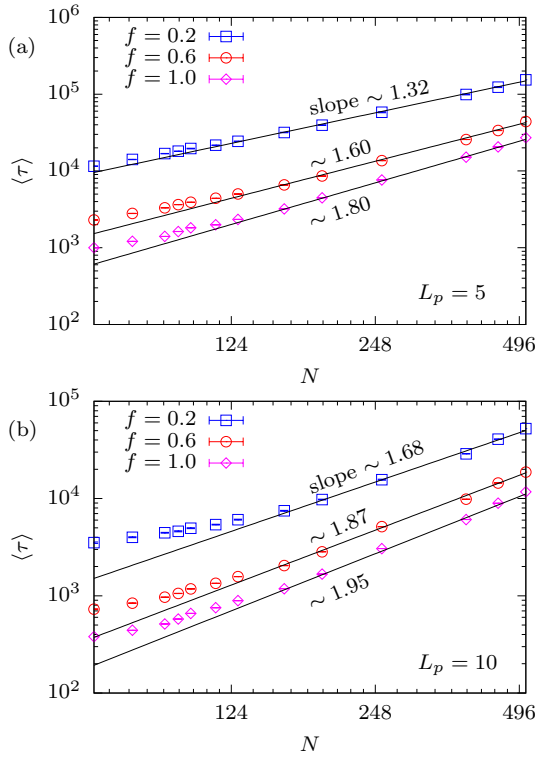


FIG. 3.  $\langle \tau \rangle$  as a function of  $N$  (in log-log scale) for three different driving forces when the polymer is translocating from an extended cylindrical pore (i.e.,  $\alpha = 0$ ) of length (a)  $L_p = 5\sigma$ , and (b)  $L_p = 10\sigma$ . The slopes mentioned in the plot are the values of the translocation exponent,  $\beta$ , defined by  $\langle \tau \rangle \sim N^\beta$ , for different driving forces.

of  $\alpha$  for various  $L_p$ .

Figure 2 shows that (i) for cylindrical pores ( $\alpha = 0^\circ$ ) the mean translocation time  $\langle \tau \rangle$  decreases strongly with pore length  $L_p$ , and (ii) for conical pores ( $\alpha > 0$ )  $\langle \tau \rangle$  decreases with  $\alpha$  for *short* pores but *increases* with  $\alpha$  for *long* pores. This behavior can be understood as a competition between two effects: (a) the widening exit increases the available configuration space for the leading segment and reduces confinement-related hindrance near the exit (entropic relief), which facilitates the final emptying for short pores; and (b) the imposed driving field in a cone decreases along the pore,  $f_{\text{ext}}(x) = f_0 d / (d + 2x \tan \alpha)$  (Eq. (4)), so an extended weak-drive region develops near the exit, making long conical pores bottleneck-limited. Because polymer translocation is a nonequilibrium process involving tension propagation and conformation changes along the chain, we do not attempt a point-particle drift-time theory; instead, the finite-size scaling analysis presented below provides the quantitative characterization of  $\langle \tau \rangle$  across  $(N, L_p, \alpha)$  and pore patterning.

*Role of attractive interactions.* In short cones, the entropic assistance dominates and  $\langle \tau \rangle$  decreases with  $\alpha$  before saturating once the exit is sufficiently wide. In long

cones, the weakening of the local drive near the exit, outweighs the entropic gain; therefore,  $\langle \tau \rangle$  *increases* with  $\alpha$ . Attractive pore–polymer interactions further amplify this effect by increasing residence near the walls and promoting side-by-side monomer arrangements that impede axial progress, again more relevant at larger  $L_p$  where the low-drive region is longer.

*Consistency with the finite-size scaling analysis.* The same geometry–drive competition is reflected in the scaling form  $\langle \tau \rangle \sim N^\gamma \mathcal{F}(L_p N^\phi)$  with  $\mathcal{F}(x) \sim x^{-p}$ : for  $\alpha = 0$ , increasing  $L_p$  increases the number of driven monomers and decreases  $\langle \tau \rangle$  (smaller  $\mathcal{F}$ ); for  $\alpha > 0$ , the weakening of the local drive near the exit with increasing  $L_p \tan \alpha$  counteracts and eventually reverses the entropic speed-up, consistent with the crossover observed in Fig. 2. The measured exponents also satisfy  $\beta \approx \gamma - (\phi p)/2$ , linking the chain-length and pore-length dependence.

## B. Effect of chain length $N$

Next, we study how  $\langle \tau \rangle$  varies with the chain length  $N$  for pores of fixed lengths  $L_p = 5\sigma$  and  $10\sigma$ . Let us first consider translocation through a cylindrical pore (i.e.,  $\alpha = 0$ ). In Figs. 3(a) and 3(b), we have plotted  $\langle \tau \rangle$  as a function of  $N$  for a polymer translocating through a cylindrical pore of lengths  $L_p = 5$  and  $10$ , respectively for various values of driving forces  $f_0 = 0.2, 0.6$  and  $1.0$ . The translocation time exponent  $\beta$  is defined as  $\tau \sim N^\beta$ . Recall that, for a flexible polymer translocating from a slit, it was found that the exponent  $\beta < 1 + \nu$ , where  $\nu$  is the size exponent [14, 16]. In 1- and 2-dimensions  $\nu = 1.0$  and  $0.75$ , respectively. It is known that the value of exponent  $\beta$  depends on many factors such as chain length, chain flexibility, driving force, friction, and pore structure. This is also observed in our simulations. For a smaller driving force  $f_0 = 0.2$ , we found that the numerical value of the exponent for pore length  $L_p = 5$  is  $\beta = 1.32$ , which is smaller than  $1 + \nu = 1.75$ . On increasing the pore length to  $L_p = 10$ , the value of the exponent becomes  $\beta = 1.68$  but still less than  $1.75$ . On increasing the driving force to  $f_0 = 0.6$ , the translocation exponent for  $L_p = 5$  is  $\beta = 1.60 < 1.75$ . However, for pore length  $L_p = 10$ , the exponent becomes  $\beta = 1.87 > 1.75$ . For a driving force  $f_0 = 1.0$ , the value of the translocation exponent for pore lengths  $L_p = 5$  and  $10$  are  $1.80$  and  $1.95$ , respectively, with both being greater than  $1.75$  but less than  $2$ .

We have seen that the translocation exponent  $\beta$  varies with the length of the extended pore. We now seek to see whether the average translocation time  $\langle \tau \rangle$  for different pore lengths  $L_p$  and the polymer chain lengths  $N$  follow some scaling. To check this, we take the scaling form for  $\langle \tau \rangle$ :

$$\langle \tau \rangle \sim N^\gamma \mathcal{F}(L_p N^\phi), \quad (6)$$

where  $\gamma$  and  $\phi$  are exponents, and  $\mathcal{F}$  is the scaling function. In Fig. 4, we have plotted  $\langle \tau \rangle/N^\gamma$  as a function of

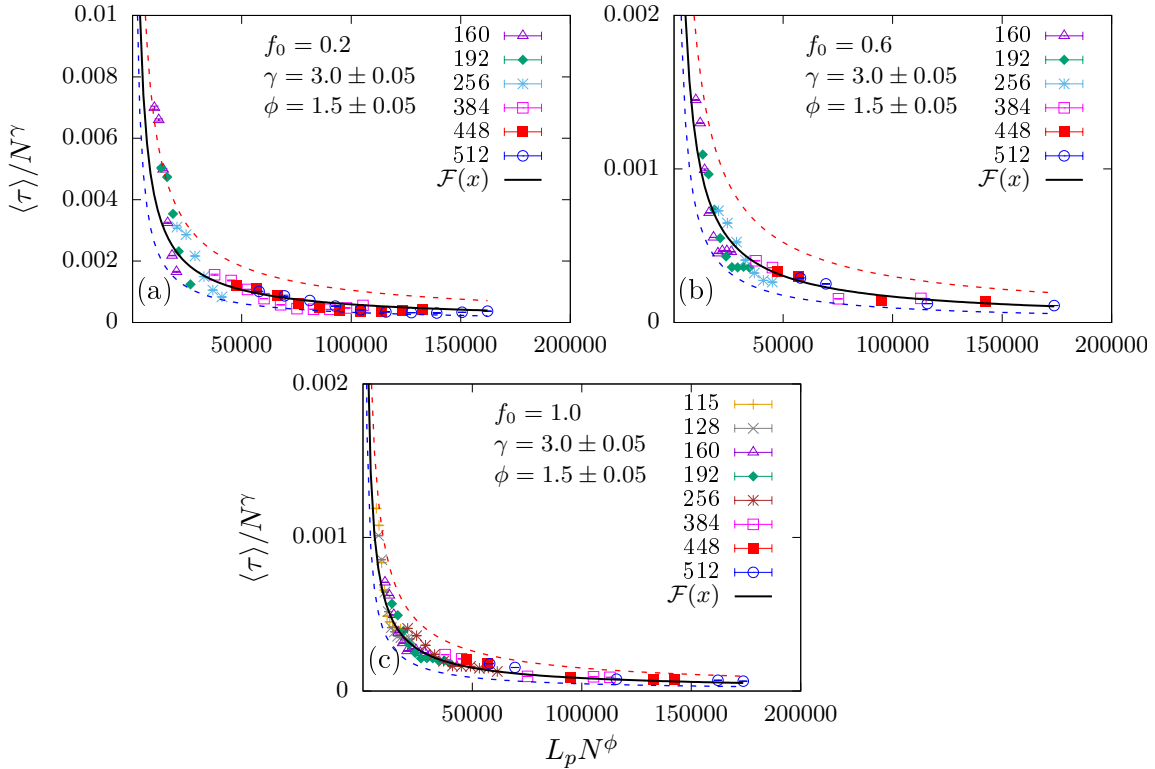


FIG. 4.  $\langle \tau \rangle / N^\gamma$  as a function of  $L_p N^\phi$  for an extended pore ( $\alpha = 0$ ) for three different driving forces (a) 0.2, (b) 0.6, and (c) 1.0. The lines are the scaling function  $\mathcal{F}(x) \sim 1/x^p$  with exponent  $p = 0.85$ . The dashed line above (below) is for exponent value  $p = 0.80$  ( $p = 0.90$ )

$L_p N^\phi$  for pore lengths  $L_p$  varying from 5 to 10 and chain lengths varying from  $N = 160$  to 512. A good data collapse is obtained for exponent values  $\gamma = 3.0 \pm 0.05$  and  $\phi = 1.50 \pm 0.05$  for three driven force values ( $f_0 = 0.2$ , 0.6, and 1.0) discussed in this paper. The scaling function follows a power law,  $\mathcal{F}(x) \sim 1/x^p$ , with a consistent exponent  $p \sim 0.85$  for each of the three forces  $f_0 = 0.2$ , 0.6, and 1.0. For reader guidance, Fig. 4(a) additionally shows dashed comparison curves generated with  $p = 0.80$  and  $p = 0.90$  to illustrate the sensitivity of the collapse to the exponent choice. We also discuss in Sec. IV how the observed set of exponents is consistent, within uncertainty, with the measured  $\beta$  via the relation  $\beta \approx \gamma - (\phi p)/2$ .

### C. Effect of pore patterning

In this sub-section, we discuss the effect of pore patterning (shown in Fig. 1) on  $\tau$  for a polymer of length  $N = 128$ . The translocation of flexible and semiflexible polymers through cylindrical and conical pores has been studied in the past [31, 34, 40, 41]. It was observed that the translocation time and its standard deviation can be used to sequence the polymer by translocating the polymer multiple times through different patterned pores. Our interest in this paper is to explore the de-

pendence of  $\tau$  on the pore length  $L_p$  of various patterned pores. We increase the pore length in such a manner that the ratio of pore patterning remains conserved. As seen in the second, third and fourth rows of Fig. 1, the ratio of repulsive pore beads (yellow bead) to attractive pore beads (blue) remains the same for three pores with pore lengths  $L_p = 5, 10$ , and 15.

In Fig. 5, we have plotted the total translocation time  $\tau$  for a flexible polymer of length  $N = 128$ , as a function of the angle of the pore apex  $\alpha$  for three different pore lengths  $L_p = 5, 10$ , and 15 at two different values of the driving force  $f_0 = 0.6$  and 1.0. The figure clearly shows that the behavior of  $\tau$  strongly depends on the type of pore and its length. For shorter pore lengths (e.g.  $L_p = 5$ ), we observe that for both force values,  $\tau$  decreases with  $\alpha$  and becomes saturated. This is true for the three types of pores studied in this paper (see Figs. 5(a) and 5(d)). Upon comparing  $\tau$  among these pores, we observed that the pore with a repulsive exit (presented by the triangles) favors faster translocation at all angles. This is followed by the pore with an attractive entrance and exit with a repulsive bead in the middle (presented by the circles), whereas the translocation is the slowest for a fully attractive pore (presented by the squares). For intermediate-length pores (that is,  $L_p = 10$ ), the translocation time  $\tau$  first increases with  $\alpha$  for the force values  $f_0 = 0.6$  and 1.0. For a fully at-

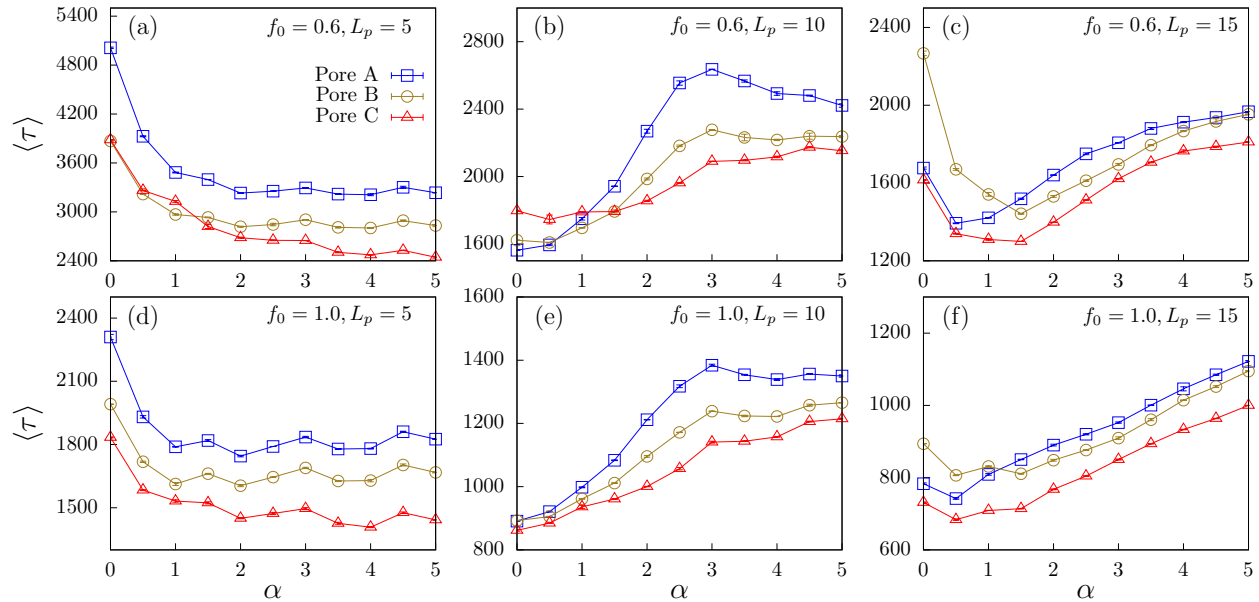


FIG. 5. Comparison of  $\tau$  vs.  $\alpha$  for three different pore sizes  $L_p = 5, 10$  and  $15$  for two different forces  $f_0 = 0.6$  and  $1.0$ . The length  $N$  of the flexible polymer chain is 128 beads.

tractive pore (see Fig. 1(a2)) it reaches a maximum at about  $\alpha \approx 3^\circ$  and then decreases as  $\alpha$  increases further. For pore types with repulsive beads, either in the middle (see Fig. 1(b2)) or at the exit (see Fig. 1(c2)), the value of  $\tau$  becomes saturated around  $\alpha \approx 3^\circ$  (see Figs. 5(b) and 5(e)). The above-mentioned feature is more pronounced for lower force values  $f_0 = 0.6$ . When the pore length increases further (e.g.  $L_p = 15$ ), the translocation time first decreases with  $\alpha$ . It reaches a minimum value at some value of  $\alpha$ , which is different for different types of pores, and then  $\tau$  increases as  $\alpha$  increases further (see Figs. 5(c) and 5(f)).

To obtain the scaling of the averaged total translocation time with pore length  $L_p$  and chain length  $N$  for patterned pores, we again use the scaling relation of the form:

$$\langle \tau \rangle \sim N^\gamma \mathcal{H}(L_p N^\phi), \quad (7)$$

where  $\phi$  and  $\gamma$  are exponents, and  $\mathcal{H}$  is the scaling function. We observe that when  $\langle \tau \rangle/N^\gamma$  is plotted as a function of  $L_p N^\phi$ , for various pore lengths  $L_p$  and chain lengths  $N$ , the data collapse to a scaling curve  $\mathcal{H}(x) \sim 1/x^q$ . The exponents  $\gamma$  and  $\phi$  are remarkably robust, showing no dependence on whether the pore is cylindrical (i.e.  $\alpha = 0$ ) or conical ( $\alpha \geq 0$ ) in shape. Adjusting the proportionality constant in the scaling function  $\mathcal{H}$ , we consistently obtain the exponent  $q \sim 0.8$  for the cylindrical pore and  $q \sim 0.6$  for the conical pore, respectively. Furthermore, the exponents do not vary much with  $f_0$ . The data collapses for  $\alpha = 0$  and  $\alpha = 3$  are shown in Figs. 6 and 7, respectively.

#### IV. DISCUSSION

We investigated driven translocation of a flexible polymer through extended pores while varying chain length  $N$ , pore length  $L_p$ , pore geometry via cone angle  $\alpha$ , and axial patterning. There are three main observations that emerge. (i) At fixed  $N$ ,  $\langle \tau \rangle$  decreases with  $\alpha$  for short pores but increases with  $\alpha$  for long pores (Fig. 2), revealing a geometry-drive competition. (ii) For cylindrical pores ( $\alpha = 0^\circ$ ),  $\langle \tau \rangle$  decreases with  $L_p$  because a longer pore hosts more monomers under a uniform drive. (iii) Finite-size scaling collapses of  $\langle \tau \rangle$  versus  $N$  and  $L_p$  are obtained with  $\langle \tau \rangle \sim N^\gamma F(L_p N^\phi)$ ; the best collapses give  $\gamma \simeq 3.0$  and  $\phi \simeq 1.5$ , with a power-law scaling function  $F(x) \sim x^{-p}$ .

The opposite trends of  $\langle \tau \rangle(\alpha)$  at small and large  $L_p$  can be understood from two coupled effects. First, the widening exit reduces the entropic confinement penalty and local wall-mediated hindrance for the leading part of the chain, which speeds up the final emptying for short pores (entropic relief). Second, in a cone the local field decreases along the pore,  $f_{\text{ext}}(x) = f_0 d/(d + 2x \tan \alpha)$  (Eq. (4)), so an extended weak-drive region develops near the exit; for long pores this slow final emptying dominates and can reverse the trend, making  $\langle \tau \rangle$  increase with  $\alpha$ . We emphasize that we use this picture only qualitatively and rely on the scaling collapses for robust quantitative statements.

Practically, these results identify two independent design levers for nanopore transport: (i) increasing  $L_p$  (at  $\alpha = 0^\circ$ ) boosts the number of driven monomers and accelerates translocation; (ii) for conical pores, small  $\alpha$  values can improve throughput via entropic assistance, but

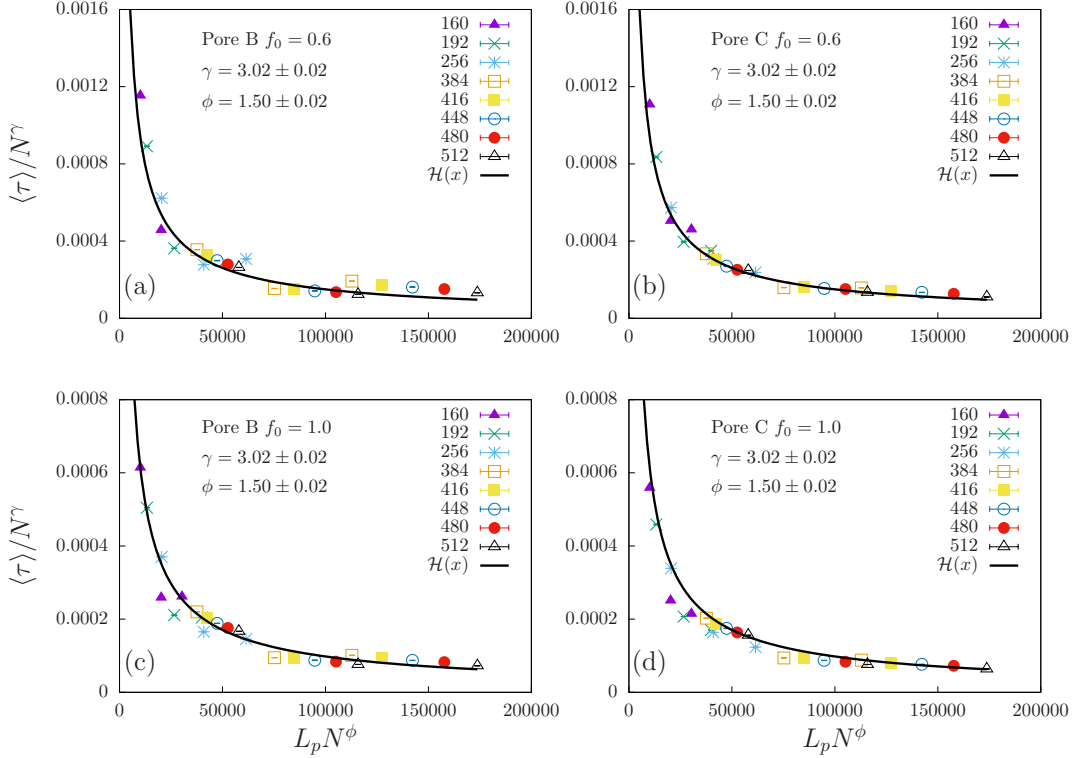


FIG. 6.  $\langle \tau \rangle / N^\gamma$  as a function of  $L_p N^\phi$  for patterned pores: Pore B and Pore C for  $\alpha = 0$  and three different pore lengths  $L_p = 5, 10$  and  $15$  and various chain lengths  $N$  as indicated in the plots. Plots (a), (b) are for force  $f_0 = 0.6$  and plots (c), (d) are for force  $f_0 = 1.0$ , respectively. The solid line represents the scaling function of the form  $\mathcal{H}(x) \sim 1/x^p$  with exponent  $p = 0.8$ .

beyond a geometry-dependent crossover the weak-field exit becomes a bottleneck. Pore patterning further modulates residence near the exit: a repulsive exit expedites release, while attractive exits prolong it, suggesting protocols for sequence-sensitive discrimination based on the full  $(L_p, \alpha)$  space.

Our  $\langle \tau \rangle(\alpha)$  crossover is consistent with cone-induced entropic driving reported by Fazli and co-workers [35, 37], where a blob-based confinement-entropy picture predicts a non-monotonic entropic bias with  $\alpha$  and a saturation for wide exits. In our driven setting, the same entropic relief operates at short  $L_p$  (decrease and saturation with  $\alpha$ ), while for large  $L_p$  the position-dependent external field in the cone dominates and can reverse the trend (increase with  $\alpha$ ). For  $\alpha = 0^\circ$ , our observation that longer pores reduce  $\langle \tau \rangle$  aligns with earlier findings that extended, fully driven segments transit faster than short pores under uniform fields.

The pair  $(\gamma, \phi) \approx (3.0, 1.5)$  provides high-quality collapses across drives. The exponent  $p$  that characterizes  $F(x) \sim x^{-p}$  is found to be of order unity; *importantly, its precise value may depend on geometry and patterning*. In particular, collapses with  $p \simeq 0.8$  (cylindrical patterned pores) and  $p \simeq 0.6$  (conical patterned pores) also provide good descriptions (Figs. 6–7). *To avoid*

*over-claiming universality*, we therefore report that  $p$  is *geometry-sensitive* in our finite ranges of  $(L_p, \alpha)$ , whereas  $(\gamma, \phi)$  are robust within uncertainties. The measured  $\beta$  from  $\langle \tau \rangle \sim N^\beta$  is consistent, within error, with the relation  $\beta \approx \gamma - (\phi p)/2$  obtained from the scaling form.

Our study is two-dimensional and neglects hydrodynamic interactions. Furthermore, we employ reduced units and a specific choice of attractive/repulsive patterns. Entrance beads are attractive by design to ensure capture. Chain lengths and pore lengths are finite and selected to balance resolution with sampling (1500–2000 successful events per point). These choices may shift the apparent crossover in  $\langle \tau \rangle(\alpha)$  and the fitted  $p$  relative to other models or experiments.

Extending the present analysis to 3D with hydrodynamic interactions, exploring broader  $(N, L_p, \alpha)$  ranges, and directly measuring spatially resolved observables (e.g., monomer waiting-time/residence profiles along the pore axis and the distribution of the final emptying time) would sharpen the geometry–drive disentanglement. It would also be instructive to vary the entrance capture condition (non-attractive entrance) and to test other patterning ratios to map out  $p(\alpha)$  more completely. Finally, comparing with experiments that can tune cone angles and patterning independently would help assess how the

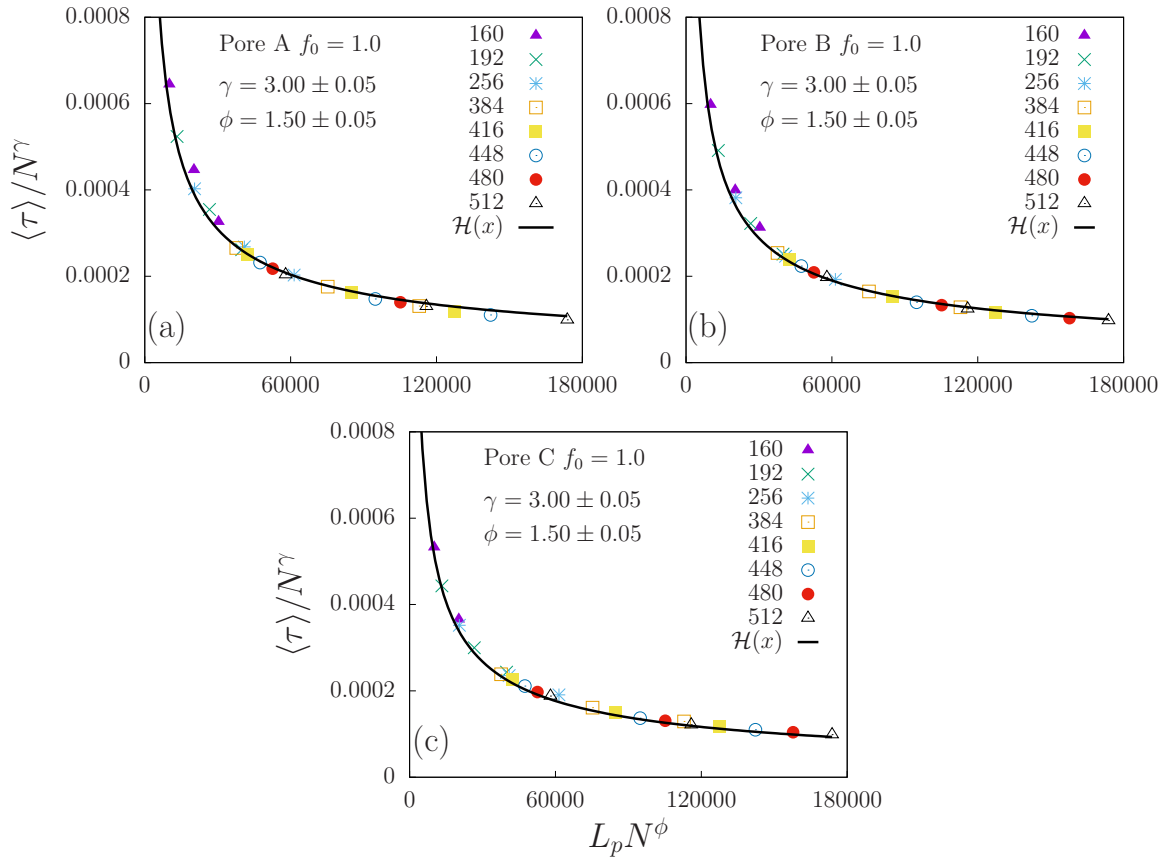


FIG. 7.  $\langle \tau \rangle / N^\gamma$  as a function of  $L_p N^\phi$  for patterned pores (a) Pore A, (b) Pore B and (c) Pore C for  $\alpha = 3^\circ$  and  $f_0 = 1.0$ . Three different pore lengths used are  $L_p = 5, 10$  and  $15$  and various chain lengths  $N$  as indicated in the plots. The solid line indicates the scaling function of the form  $\mathcal{H}(x) \sim 1/x^p$  with exponent  $p = 0.6$ .

crossover scale depends on solvent, voltage, and surface chemistry.

## V. ACKNOWLEDGEMENT

The authors acknowledge the IISER Mohali computing facility for providing the necessary resources and support for this work.

---

[1] B. Alberts, D. Bray, J. Lewis, M. Raff, K. Roberts, and J. Watson, *Molecular Biology of the Cell*, 4th ed. (Garland, 2002).

[2] M. van der Laan, M. Meinecke, J. Dudek, D. P. Hutz, M. Lind, I. Perschil, B. Guiard, R. Wagner, N. Pfanner, and P. Rehling, *Nature cell biology* **9**, 1152 (2007).

[3] H. Salman, D. Zbaida, Y. Rabin, D. Chatenay, and M. Elbaum, *Proceedings of the National Academy of Sciences* **98**, 7247 (2001).

[4] Y.-L. Ying, Z.-L. Hu, S. Zhang, Y. Qing, A. Fragasso, G. Maglia, A. Meller, H. Bayley, C. Dekker, and Y.-T. Long, *Nat. Nanotechnol.* **17**, 1136 (2022).

[5] J. J. Kasianowicz, E. Brandin, D. Branton, and D. W. Deamer, *Proceedings of the National Academy of Sciences* **93**, 13770 (1996).

[6] M. Muthukumar, *Annu. Rev. Biophys. Biomol. Struct.* **36**, 435 (2007).

[7] M. Muthukumar, *Polymer Translocation* (1st ed.). (CRC Press., 2011).

[8] W. Sung and P. Park, *Physical review letters* **77**, 783 (1996).

[9] V. V. Palyulin, T. Ala-Nissila, and R. Metzler, *Soft matter* **10**, 9016 (2014).

[10] P. Rowghanian and A. Y. Grosberg, *The Journal of Physical Chemistry B* **115**, 14127 (2011).

[11] T. Sakaue, *Physical Review E* **76**, 021803 (2007).

[12] Y. Kantor and M. Kardar, *Physical Review E* **69**, 021806 (2004).

[13] J. Dubbeldam, A. Milchev, V. Rostiashvili, and T. A. Vilgis, *Europhysics Letters* **79**, 18002 (2007).

[14] T. Ikonen, A. Bhattacharya, T. Ala-Nissila, and W. Sung, *Physical Review E* **85**, 051803 (2012).

[15] M. Muthukumar, *The Journal of Chemical Physics* **111**, 10371 (1999).

[16] T. Ikonen, A. Bhattacharya, T. Ala-Nissila, and W. Sung, *The Journal of chemical physics* **137**, 085101 (2012).

[17] J. Sarabadani, T. Ikonen, and T. Ala-Nissila, *The Journal of Chemical Physics* **141**, 214907 (2014).

[18] J. Sarabadani and T. Ala-Nissila, *Journal of Physics: Condensed Matter* **30**, 274002 (2018).

[19] J. L. A. Dubbeldam, V. G. Rostiashvili, A. Milchev, and T. A. Vilgis, *Phys. Rev. E* **85**, 041801 (2012).

[20] K. Chen, I. Jou, N. Ermann, M. Muthukumar, U. F. Keyser, and N. A. Bell, *Nature Physics* **17**, 1043 (2021).

[21] A. Milchev, *Journal of Physics: Condensed Matter* **23**, 103101 (2011).

[22] J. Chuang, Y. Kantor, and M. Kardar, *Physical Review E* **65**, 011802 (2001).

[23] K. Luo, T. Ala-Nissila, S.-C. Ying, and A. Bhattacharya, *Physical Review Letters* **99**, 148102 (2007).

[24] M. Doi, S. F. Edwards, and S. F. Edwards, *The theory of polymer dynamics*, Vol. 73 (oxford university press, 1988).

[25] A. Storm, J. Chen, X. Ling, H. Zandbergen, and C. Dekker, *Nature materials* **2**, 537 (2003).

[26] M. Wanunu and A. Meller, *Nano letters* **7**, 1580 (2007).

[27] P. Chen, J. Gu, E. Brandin, Y.-R. Kim, Q. Wang, and D. Branton, *Nano letters* **4**, 2293 (2004).

[28] W.-J. Lan, D. A. Holden, and H. S. White, *Journal of the American Chemical Society* **133**, 13300 (2011).

[29] Q. Liu, H. Wu, L. Wu, X. Xie, J. Kong, X. Ye, and L. Liu, *PLoS one* **7**, e46014 (2012).

[30] K. Luo, T. Ala-Nissila, S.-C. Ying, and A. Bhattacharya, *Physical Review E* **78**, 061918 (2008).

[31] J. A. Cohen, A. Chaudhuri, and R. Golestanian, *Physical Review X* **2**, 021002 (2012).

[32] J. A. Cohen, A. Chaudhuri, and R. Golestanian, *The Journal of chemical physics* **137**, 204911 (2012).

[33] H. H. Katkar and M. Muthukumar, *The Journal of chemical physics* **148**, 024903 (2018).

[34] R. Kumar, A. Chaudhuri, and R. Kapri, *The Journal of chemical physics* **148**, 164901 (2018).

[35] N. Nikoofard, H. Khalilian, and H. Fazli, *The Journal of Chemical Physics* **139**, 074901 (2013).

[36] N. Nikoofard, S. M. Hoseinpoor, and M. Zahedifar, *Physical Review E* **90**, 062603 (2014).

[37] N. Nikoofard and H. Fazli, *Soft Matter* **11**, 4879 (2015).

[38] A. Sharma, R. Kapri, and A. Chaudhuri, *Scientific Reports* **12**, 19081 (2022).

[39] A. Sharma, *Physica Scripta* **99**, 055025 (2024).

[40] G. Upadhyay, R. Kapri, and A. Chaudhuri, *Eur. Phys. J. E* **47**, 23 (2024).

[41] G. Upadhyay, R. Kapri, and A. Chaudhuri, *J. Phys.: Condens. Matter* **36**, 185101 (2024).

[42] G. S. Grest and K. Kremer, *Physical Review A* **33**, 3628 (1986).

[43] A. P. Thompson, H. M. Aktulga, R. Berger, D. S. Bolintineanu, W. M. Brown, P. S. Crozier, P. J. in't Veld, A. Kohlmeyer, S. G. Moore, T. D. Nguyen, *et al.*, *Computer Physics Communications* **271**, 108171 (2022).